Journal of Computational and Applied Mathematics 233 (2010) 3103–3112

Contents lists available at ScienceDirect

Journal of Computational and Applied Mathematics

journal homepage: www.elsevier.com/locate/cam

# Adaptive *hp*-FEM with dynamical meshes for transient heat and moisture transfer problems

Pavel Solin [a,b,*], Lenka Dubcova [b], Jaroslav Kruis [c]

[a] *Department of Mathematics and Statistics, University of Nevada, Reno, USA*
[b] *Institute of Thermomechanics, Dolejskova 5, Prague, Czech Republic*
[c] *Faculty of Civil Engineering, Czech Technical University, Prague, Czech Republic*

ARTICLE INFO

*Article history:*
Received 21 May 2009
Received in revised form 8 July 2009

*MSC:*
65M50
65M60
80M10

*Keywords:*
Multiphysics problems
Heat and moisture transfer
Higher-order methods
*hp*-FEM
Space–time adaptivity
Dynamical meshes
Open source software

ABSTRACT

We are concerned with the time-dependent multiphysics problem of heat and moisture transfer in the context of civil engineering applications. The problem is challenging due to its multiscale nature (temperature usually propagates orders of magnitude faster than moisture), different characters of the two fields (moisture exhibits boundary layers which are not present in the temperature field), extremely long integration times (30 years or more), and lack of viable error control mechanisms. In order to solve the problem efficiently, we employ a novel multimesh adaptive higher-order finite element method (*hp*-FEM) based on dynamical meshes and adaptive time step control. We investigate the possibility to approximate the temperature and humidity fields on individual dynamical meshes equipped with mutually independent adaptivity mechanisms. Numerical examples related to a realistic nuclear reactor vessel simulation are presented.



## 1. Introduction

Many nuclear power plants across Europe and the US approach the end of their service life. However, the cost of decommissioning a power plant is extremely high and therefore the prolongation of serviceability is desirable. For this, the power plant has to undergo a large amount of tests and fulfil severe criteria. Some of these involve a detailed computational analysis of the reactor vessel which has to cover the entire life span of the vessel (more than 30 years). It includes complex mechanical and transport processes to be modeled using coupled hydro-thermo-mechanical analysis based on the finite element method. In this paper, we restrict ourselves to the hydro-thermal part of the model.

The transient coupled analysis of concrete structures during long periods of time is extremely difficult for several reasons:

- In order to capture the transient phenomena with sufficient accuracy, one needs to employ a very fine mesh, which results in large matrix problems.
- The time increment must be much smaller than in creep or heat transfer analyses since it is limited by several physical processes simultaneously. The large number of unknowns combined with the short time step lead to extremely large CPU times and memory requirements. In the case of 30 years analysis with one day time increment, nearly 11,000 time steps have to be done [1].

* Corresponding author at: Department of Mathematics and Statistics, University of Nevada, Reno, USA. Tel.: +1 775 848 7892.
*E-mail address:* solin@unr.edu (P. Solin).

0377-0427/$ – see front matter 
doi:10.1016/j.cam.2009.07.025

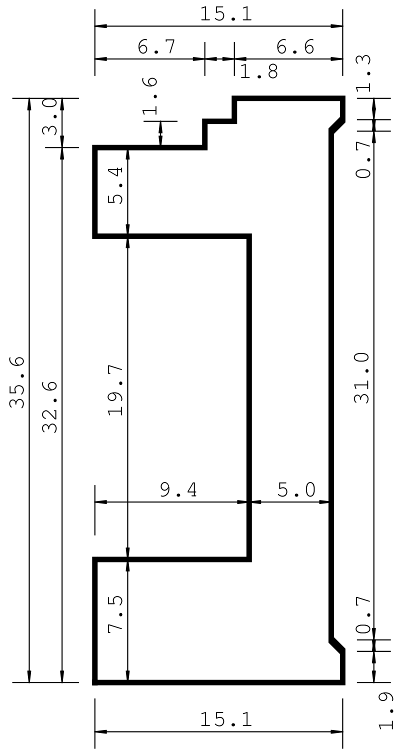


**Fig. 1.** Geometry of the reactor vessel (all measures are in meters).

- The system matrix often is nonsymmetric and indefinite due to material models of coupled heat and moisture transfer [2,3,15]. Nonsymmetric and/or indefinite matrices exclude efficient storage and solution methods that are available for symmetric matrices.
- The lack of error estimates for multiphysics problems makes it extremely difficult to assess the accuracy of the computed results. In practice, most computations of heat and moisture transfer in concrete are missing information about their accuracy.

While the efficiency and storage issues mentioned above can be alleviated to some extent by the application of domain decomposition methods [4] and parallel computers, the approximation error cannot be controlled without error estimation and automatic adaptivity.

### 1.1. Adaptive hp-FEM on dynamical meshes

As an alternative, we present a novel space and time adaptive higher-order finite element method (*hp*-FEM) [5–7] which employs fully automatically small low-degree elements on moving fronts and large high-degree elements where the solution is smooth without significant local changes. Because of large qualitative differences in the behavior of the temperature and moisture fields, we can approximate them on individual meshes that evolve in time independently of each other. The local *hp*-mesh refinements "travel" along with the moving fronts. We explain the basic ideas of the methodology and present numerical examples where the space–time adaptive *hp*-FEM is compared to space–time adaptive low-order FEM. The model is implemented using Hermes,[1] an open source GPL-licensed C++/Python library for rapid prototyping of space and space–time adaptive *hp*-FEM solvers.

## 2. The multiphysics model

The vessel is made of prestressed concrete, it is approximately 36 m high and the thickness of the walls varies between 5 and 7.5 m. The concrete is assumed to be homogeneous and isotropic. For this simulation, the vessel is assumed to be perfectly axisymmetric, although in reality there are small-scale features such as vents that make it nonsymmetric. The situation is illustrated in Fig. 1.

1 http://hpfem.org/.

The unknown variables are the temperature $T$ [K], and relative humidity $w$ [-]. The corresponding gradients are denoted by $\boldsymbol{g}^{[T]}$ [K/m] and $\boldsymbol{g}^{[w]}$ [1/m], respectively, and the corresponding fluxes by $\boldsymbol{q}^{[T]}$ [J/m$^2$/s] and $\boldsymbol{q}^{[w]}$ [kg/m$^2$/s]. The heat flux obeys the Fourier law,

$$\boldsymbol{q}^{[T]}_{\text{Fourier}} = -\boldsymbol{D}^{[TT]}\boldsymbol{g}^{[T]}. \tag{1}$$

The moisture flux is described by the Fick law,

$$\boldsymbol{q}^{[w]}_{\text{Fick}} = -\boldsymbol{D}^{[ww]}\boldsymbol{g}^{[w]}. \tag{2}$$

Coupling between the fluxes is done using the Soret flux,

$$\boldsymbol{q}^{[w]}_{\text{Soret}} = -\boldsymbol{D}^{[wT]}\boldsymbol{g}^{[T]}, \tag{3}$$

and the Dufour flux,

$$\boldsymbol{q}^{[T]}_{\text{Dufour}} = -\boldsymbol{D}^{[Tw]}\boldsymbol{g}^{[w]}\,. \tag{4}$$

The total heat and moisture fluxes have the form

$$\boldsymbol{q}^{[T]} = -\boldsymbol{D}^{[TT]}\boldsymbol{g}^{[T]} - \boldsymbol{D}^{[Tw]}\boldsymbol{g}^{[w]}, \tag{5}$$

$$\boldsymbol{q}^{[w]} = -\boldsymbol{D}^{[wT]}\boldsymbol{g}^{[T]} - \boldsymbol{D}^{[ww]}\boldsymbol{g}^{[w]}. \tag{6}$$

In the case of a homogeneous and isotropic material, the matrices of material conductivities $\boldsymbol{D}^{[TT]}$, $\boldsymbol{D}^{[Tw]}$, $\boldsymbol{D}^{[wT]}$ and $\boldsymbol{D}^{[ww]}$ can be replaced with scalars, and Eqs. (5), (6) reduce to

$$\boldsymbol{q}^{[T]} = -d^{[TT]}\boldsymbol{g}^{[T]} - d^{[Tw]}\boldsymbol{g}^{[w]}, \tag{7}$$

$$\boldsymbol{q}^{[w]} = -d^{[wT]}\boldsymbol{g}^{[T]} - d^{[ww]}\boldsymbol{g}^{[w]}. \tag{8}$$

The scalar conductivities have the following units: $d^{[TT]}$ [J/K/m/s], $d^{[Tw]}$ [J/m/s], $d^{[wT]}$ [kg/K/m/s], $d^{[ww]}$ [kg/m/s].

The balance equations of heat and moisture without source terms have the form

$$\frac{\partial \rho u}{\partial t} + \operatorname{div} \boldsymbol{q}^{[T]} = 0, \qquad \frac{\partial \rho c}{\partial t} + \operatorname{div} \boldsymbol{q}^{[w]} = 0, \tag{9}$$

where $\rho$ is the total density, $u$ is the specific internal energy and $c$ is the mass concentration of moisture [2]. The last quantity is the ratio of the weight of water and the weight of the whole system. After substitution of the fluxes (7), (8) into (9) and rearrangement of the time derivatives, the balance equations for isotropic and homogeneous materials have the form

$$c^{[TT]}\frac{\partial T}{\partial t} + c^{[Tw]}\frac{\partial w}{\partial t} - d^{[TT]}\Delta T - d^{[Tw]}\Delta w = 0, \tag{10}$$

$$c^{[wT]}\frac{\partial T}{\partial t} + c^{[ww]}\frac{\partial w}{\partial t} - d^{[wT]}\Delta T - d^{[ww]}\Delta w = 0. \tag{11}$$

Coefficients $c^{[TT]}$, $c^{[Tw]}$, $c^{[wT]}$, $c^{[ww]}$ express capacity properties. For example, $c^{[TT]}$ is the specific heat capacity. In the following, we assume that the parameters $c^{[Tw]}$ and $c^{[wT]}$ are zero, which is the usual case. Even if they were nonzero, $\partial w/\partial t$ could be eliminated from (10) and $\partial T/\partial t$ from (11) using a suitable linear combination of (10), (11). Thus the final form of the equations to be solved is

$$c^{[TT]}\frac{\partial T}{\partial t} - d^{[TT]}\Delta T - d^{[Tw]}\Delta w = 0, \tag{12}$$

$$c^{[ww]}\frac{\partial w}{\partial t} - d^{[wT]}\Delta T - d^{[ww]}\Delta w = 0. \tag{13}$$

*Time-dependent boundary conditions:*

The boundary $\partial\Omega$ is split into three disjoint parts: $\Gamma_S$ (axis of symmetry), $\Gamma_R$ (reactor wall), and $\Gamma_E$ (exterior wall). On $\Gamma_S$, one prescribes zero Neumann conditions for both $T$ and $w$:

$$\frac{\partial T}{\partial \boldsymbol{n}} = 0, \qquad \frac{\partial w}{\partial \boldsymbol{n}} = 0, \tag{14}$$

where $\boldsymbol{n}$ is the unit normal vector to $\partial\Omega$.

On the reactor wall $\Gamma_R$, one prescribes a Dirichlet condition for the temperature $T = \tilde{T}$ and a zero normal moisture flux

$$\boldsymbol{q}^{[w]} \cdot \boldsymbol{n} = \left(-d^{[wT]}\boldsymbol{g}^{[T]} - d^{[ww]}\boldsymbol{g}^{[w]}\right) \cdot \boldsymbol{n} = -d^{[wT]}\frac{\partial T}{\partial \boldsymbol{n}} - d^{[ww]}\frac{\partial w}{\partial \boldsymbol{n}} = 0.$$

Here, $\tilde{T}$ is a prescribed temperature. It is time dependent and it corresponds to a linear temperature increase from $T_0 = 293.15$ K to $T_{\max} = 550$ K in 24 h.

On the exterior wall $\Gamma_E$, we prescribe the Newton boundary conditions

$$\boldsymbol{q}^{[T]} \cdot \boldsymbol{n} = \kappa^{[TT]}(T - T_{\text{ext}}) + \kappa^{[Tw]}(w - w_{\text{ext}}), \tag{15}$$

$$\boldsymbol{q}^{[w]} \cdot \boldsymbol{n} = \kappa^{[wT]}(T - T_{\text{ext}}) + \kappa^{[ww]}(w - w_{\text{ext}}), \tag{16}$$

where $\kappa^{[TT]}$, $\kappa^{[Tw]}$, $\kappa^{[wT]}$ and $\kappa^{[ww]}$ are transmission coefficients, $T_{\text{ext}}$ is the temperature of the environment surrounding the structure and $w_{\text{ext}}$ is the relative humidity of the environment surrounding the structure. We will assume that $\kappa^{[Tw]} = \kappa^{[wT]} = 0$, which is the common case. Then conditions (15), (16) simplify to:

$$\boldsymbol{q}^{[T]} \cdot \boldsymbol{n} = -d^{[TT]}\frac{\partial T}{\partial \boldsymbol{n}} - d^{[Tw]}\frac{\partial w}{\partial \boldsymbol{n}} = \kappa^{[TT]}(T - T_{\text{ext}}), \tag{17}$$

$$\boldsymbol{q}^{[w]} \cdot \boldsymbol{n} = -d^{[wT]}\frac{\partial T}{\partial \boldsymbol{n}} - d^{[ww]}\frac{\partial w}{\partial \boldsymbol{n}} = \kappa^{[ww]}(w - w_{\text{ext}}). \tag{18}$$

Condition (18) is usually written in the form

$$\boldsymbol{q}^{[w]} \cdot \boldsymbol{n} = \beta(p - p_{\text{ext}}), \tag{19}$$

where $p$ is the water vapor pressure, $p_{\text{ext}}$ the water vapor pressure of the surrounding environment and $\beta$ the convection mass transfer coefficient. The relation between vapor pressure and the relative humidity $w$ has the form

$$w = \frac{p}{p_s(T)}, \tag{20}$$

where $p_s(T)$ is the water vapor saturation pressure. Substitution of (20) into (19) leads to the condition

$$\boldsymbol{q}^{[w]} \cdot \boldsymbol{n} = \beta(p_s(T)w - p_{s,ext}(T_{\text{ext}})w_{\text{ext}}) = \beta p_s(w - w_{\text{ext}}). \tag{21}$$

In the application discussed in this paper, the temperature of the structure $T$ and the temperature of the surrounding environment $T_{\text{ext}}$ lie within a range where the dependence of $p_s$ on the temperature can be neglected (otherwise, the problem would be nonlinear).

*Initial condition:*

Initially we assume a uniform temperature $T_0 = 293.15$ K and uniform relative humidity $w(0) = 50\%$.

## 3. Rothe's method and adaptive *hp*-FEM on dynamical meshes

Rothe's method is a natural counterpart of the widely used Method of Lines (MOL). Recall that the MOL performs discretization in space while keeping the time variable continuous, which leads to a system of ODEs in time. Rothe's method, on the contrary, preserves the continuity of the spatial variable while discretizing time. In every time step, an evolutionary PDE is approximated by means of one or more time-independent ones. The number of time-independent equations per time step is proportional to the order of accuracy of the time discretization method. For example, when employing the implicit Euler method, one has to solve one time-independent PDE per time step. Rothe's method is fully equivalent to the MOL if no adaptivity in space or time takes place, but it provides a better setting for the application of spatially adaptive algorithms. The spatial discretization error can be controlled by solving the time-independent equations adaptively, and the size of the time step can be adjusted using standard ODE techniques [8–10].

For the sake of clarity, let us illustrate our application of Rothe's method using implicit Euler discretization with a constant time step $\Delta t > 0$ (later we will switch to a higher-order method with adaptive time step). Approximating

$$\frac{\partial T}{\partial t} \approx \frac{T^{n+1} - T^n}{\Delta t}, \qquad \frac{\partial w}{\partial t} \approx \frac{w^{n+1} - w^n}{\Delta t},$$

Eqs. (12), (13) become

$$c^{[TT]}\frac{T^{n+1}}{\Delta t} - d^{[TT]}\Delta T^{n+1} - d^{[Tw]}\Delta w^{n+1} = c^{[TT]}\frac{T^n}{\Delta t}, \tag{22}$$

$$c^{[ww]}\frac{w^{n+1}}{\Delta t} - d^{[wT]}\Delta T^{n+1} - d^{[ww]}\Delta w^{n+1} = c^{[ww]}\frac{w^n}{\Delta t}. \tag{23}$$

Here the initial condition $u^0(\mathbf{x})$ and the right-hand side $f^{n+1}(\mathbf{x})$ are exact, $u^n$ is known, and $u^{n+1}$ needs to be computed. Weak formulation of Eq. (22) is derived in a standard way.

Let us denote by $\tau_0$ a uniform coarse mesh covering the computational domain $\Omega$. This mesh is used as the initial mesh for automatic adaptivity in every time step. The first approximation $u^1(\mathbf{x}) \approx u(\mathbf{x}, \Delta t_1)$ is computed adaptively in $k_1$ steps, starting from the mesh $\tau_0$ and using intermediate approximations $u^{1,1}, u^{1,2}, \ldots, u^{1,k_1} = u^1$ on meshes $\tau_{1,1}, \tau_{1,2}, \ldots, \tau_{1,k_1} = \tau_1$. The number $k_1$ depends on a user-defined tolerance $TOL_s$ for the spatial error.

At the beginning of the $(n+1)$st time step, the approximation $u^n$ is defined on a locally refined mesh $\tau_n$ that was constructed adaptively in the $n$th step. (The only exception is $u^0$ which is defined on the coarse mesh $\tau_0$.) The unknown $u^{n+1}$ is computed adaptively in $k_{n+1}$ steps starting from the mesh $\tau_0$ and using intermediate approximations $u^{n+1,1}$, $u^{n+1,2}$, $\ldots, u^{n+1,k_{n+1}} = u^{n+1}$ on meshes $\tau_{n+1,1}, \tau_{n+1,2}, \ldots, \tau_{n+1,k_{n+1}} = \tau_{n+1}$. Note that in the $m$th adaptivity step, the functions $u^n$ and $u^{n+1,m}$ are defined on different meshes $\tau_n$ and $\tau_{n+1,m}$ which were obtained from the coarse mesh $\tau_0$ through finite sequences of mutually independent local refinements. In order to perform assembling in this situation, we developed a technique that we call *multimesh hp*-FEM [5,11].

To the best of our knowledge, analytical error estimates for the multiphysics problem we study are not available. See, for example, [12,13] and the references therein for the state-of-the-art a posteriori error estimation for elliptic problems. Therefore, we guide the automatic *hp*-adaptivity using a robust computational a posteriori error estimate based on the approximation on a globally *hp*-refined mesh [7]. It is worth mentioning that our implementation of adaptive *hp*-FEM allows for arbitrary-order hanging nodes in the mesh, which makes our method much more efficient compared to methods working with regular meshes [6].

## 4. Adaptive time integration

Adaptive time integration is carried out using a pair of second-order BDF formulas BDF2a and BDF2b [14]. This method is second-order accurate and very efficient since both BDF2a and BFD2b employ the same stages. In every time step, the difference between the pair of results provides an estimate of the local truncation error that is used to adapt the time step. The scheme of the adaptive algorithm is as follows:

On each time level do {

1. calculate a solution using BDF2a
2. calculate a solution using BDF2b
3. calculate error estimate $e_k$ using the difference of the two solutions
4. if $e_k > TOL_t$ repeat process with new time step $\tau_k = 0.99\, TOL_t\, \tau_k / e_k$
5. if $e_k < TOL_t$ proceed to the time level $k+1$ with new time step

$$\tau_{k+1} = \left(\frac{e_{k-1}}{e_k}\right)^{k_P} \left(\frac{TOL_t}{e_k}\right)^{k_I} \left(\frac{e_{k-1}^2}{e_k e_{k-2}}\right)^{k_D} \tau_k.$$

}

The PID controller (last formula in the algorithm above) is used to adjust the time step smoothly. This is the standard method used in automatic control, robotics and related fields,

## 5. Numerical examples

In this section we use the problem described in Section 2 to compare the performance of three adaptive methods: (a) *h*-adaptive FEM with quadratic elements, (b) adaptive *hp*-FEM where both fields are approximated on the same mesh (standard *hp*-FEM), and (c) adaptive *hp*-FEM where the temperature and humidity are approximated on individual meshes. It should be noted that we dropped *h*-adaptive FEM with linear elements from this comparison due to its excessive CPU times, and also that we dropped non-adaptive computations on fixed meshes.

To the last point, such comparison would be very interesting since non-adaptive computations with fixed uniform fine meshes still prevail in practical engineering computations of transient processes. However, in practice these are virtually never accompanied with an a posteriori error estimate, and we believe that it is impossible to compare methods that use a posteriori error control with methods that do not. Even if a non-adaptive computation was accompanied with an a posteriori error information, in our opinion it still cannot be compared to an adaptive method since the former does not invest any effort into controlling the error while the latter does, and work and CPU time used by a method to control the error should not be counted to its disadvantage.

We use the following material parameters (see [2]): $d^{[TT]} = 2.1$ [J/K/m/s], $d^{[Tw]} = 2.37 \times 10^{-2}$ [J/m/s], $d^{[wT]} = 1.78 \times 10^{-10}$ [kg/K/m/s], $d^{[ww]} = 3.02 \times 10^{-8}$ [kg/m/s], $c^{[TT]} = 2.18 \times 10^{6}$ [J/K/m$^3$], $c^{[Tw]} = 0$, $c^{[wT]} = 0$, $c^{[ww]} = 2.49 \times 10^{1}$ [kg/m$^3$]. The transition coefficients have the values $\kappa^{[TT]} = 25$ [J/K/m$^2$/s], $\kappa^{[Tw]} = 0$, $\kappa^{[wT]} = 0$, $\kappa^{[ww]} = 1.84 \times 10^{-7}$ [kg/m$^2$/s]. Boundary and initial conditions were defined in Section 2.

Let us begin with showing the temperature and moisture distribution in the vessel after 30 years in Fig. 2.

In order to compare the three methods fairly, we established a control quantity of interest to be the total moisture content in the vessel after 30 years of operation of the power plant, and we used an overkill method of solution (with extremely fine resolution both in space and time) to calculate as accurate reference value as possible.

Each of the three adaptive algorithms in consideration contains a pair of tolerance parameters $TOL_s$ and $TOL_t$ (see Sections 3 and 4) that serve as stopping criteria for the spatial adaptivity in every time step and for the adaptive control of the

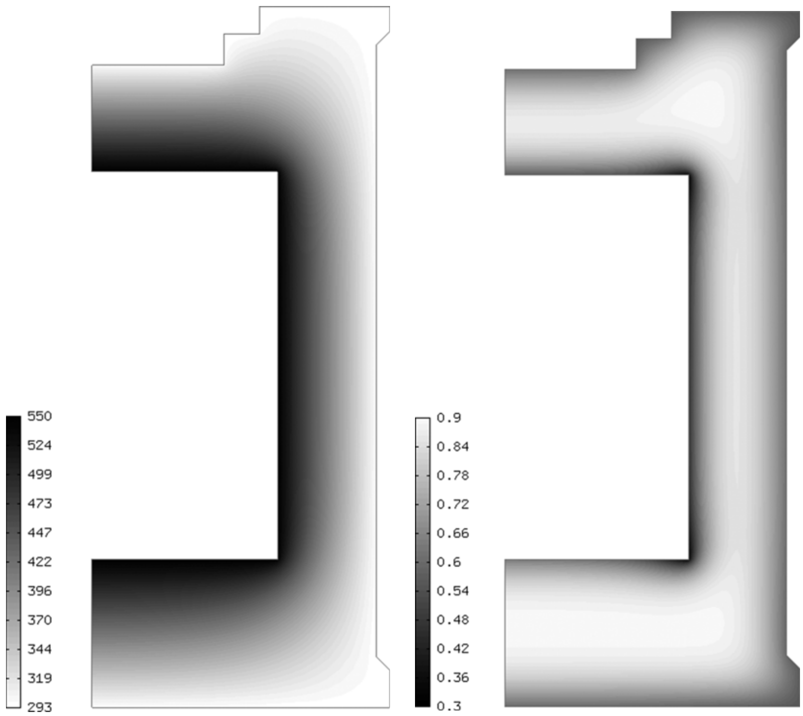


**Fig. 2.** Temperature and moisture distribution in the vessel after 30 years.

time step, respectively. Typically, these parameters are set to some default values at the beginning of computation and they imply some accuracy for the final results. However, we faced an inverse problem: In order to compare the three methods on the same level of accuracy (in terms of the quantity of interest at the time level of 30 years), we had to go through many trial and error computations using various values of these parameters. Some details about the final computations leading to the same accuracy in the quantity of interest are presented in the following.

*Adaptive h-FEM with quadratic elements*

Fig. 3 shows a series of finite element meshes generated by the *h*-adaptive FEM with quadratic elements. The reader can see that both mesh refinement and coarsening took place over the 30 year period.

*Standard adaptive hp-FEM (same meshes for temperature and moisture)*

Fig. 4 shows an analogous series of meshes generated by the standard (single-mesh) *hp*-adaptive FEM.

*Adaptive multimesh hp-FEM (with individual meshes for temperature and moisture)*

In the multimesh *hp*-FEM we allow the meshes for the temperature and moisture fields to be different and to evolve in time independently of each other. If the two fields exhibit significantly different behaviors, then this approach can save many degrees of freedom. It is worth mentioning that despite the meshes are different, the discretization is monolithic (no operator splitting takes place)—see, e.g., [11]. Figs. 5 and 6 show the corresponding series of temperature and moisture meshes, respectively.

*Comparison in terms of DOF and CPU time requirements*

Lastly let us compare the performance of the three adaptive methods in terms of degrees of freedom (DOF) and CPU time requirements. Let us remind the reader that the three comparisons are fair in the sense that all three methods achieved the same accuracy in a given quantity of interest (total contents of moisture in the vessel after 30 years).

The reader can see in Fig. 7 that the *h*-FEM with quadratic elements consumes many more DOF than both versions of the adaptive *hp*-FEM. This is a standard observation that will not surprise anyone. It is more interesting to see that the difference between the standard and multimesh *hp*-FEM is more significant during the first approximate 15 years than in the second half of the time interval. This is due to the fact that in the early stage of the computation, the moisture develops a thin boundary layer which is not present in the temperature fields (see Figs. 5 and 6). Therefore the meshes for temperature and moisture are very different during the initial stage of the computation. Later, as the moisture layers become smeared, these differences vanish, and after 30 years both meshes become very similar (compare the right-most parts of Figs. 5 and 6).

The differences in the discrete problem sizes from Fig. 7 yield different CPU time requirements of the three methods, as shown in Fig. 8.

Here, the reader may notice that the difference between the standard and multimesh *hp*-FEM is less significant than their difference in terms of DOF. This is due to numerical integration that is more involved in the multimesh case [11] (we hope to be able to optimize it in the future). The evolution of the time step for all three computations is shown in Fig. 9.

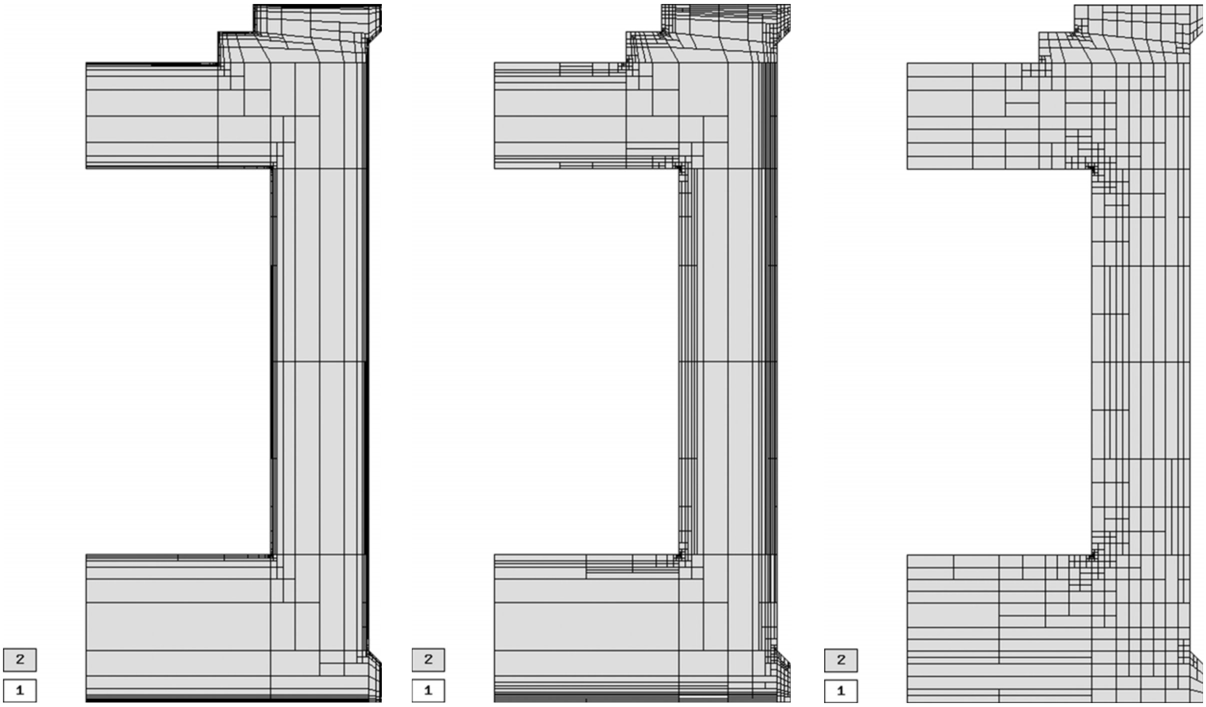


**Fig. 3.** Adaptive *h*-FEM with quadratic elements (mesh after 1 month, 1 year, and 30 years).

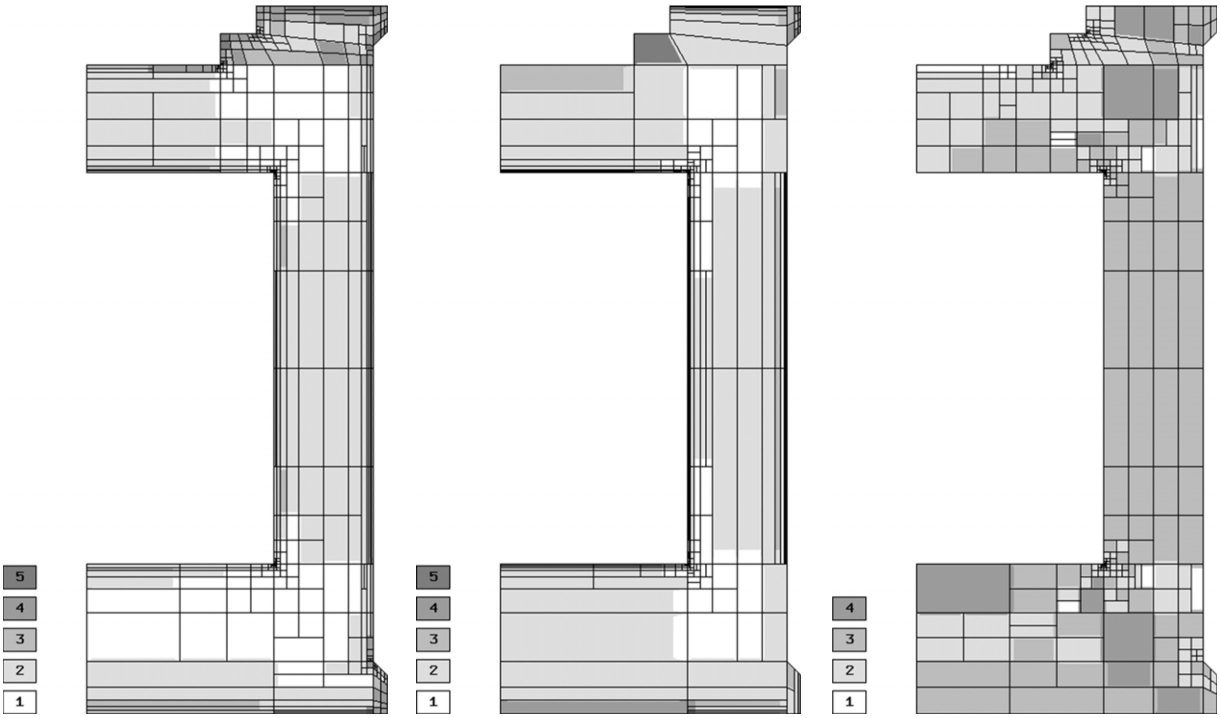


**Fig. 4.** Standard adaptive (single-mesh) *hp*-FEM (mesh after 1 month, 1 year, and 30 years).

## 6. Conclusion and outlook

We presented a novel space–time adaptive *hp*-FEM algorithm based on dynamical meshes and equipped with adaptive control of the time step. The method is higher-order accurate and adaptive in both space and time, and it is capable of approximating both physical fields, the temperature and the moisture, on individual meshes that can evolve in time

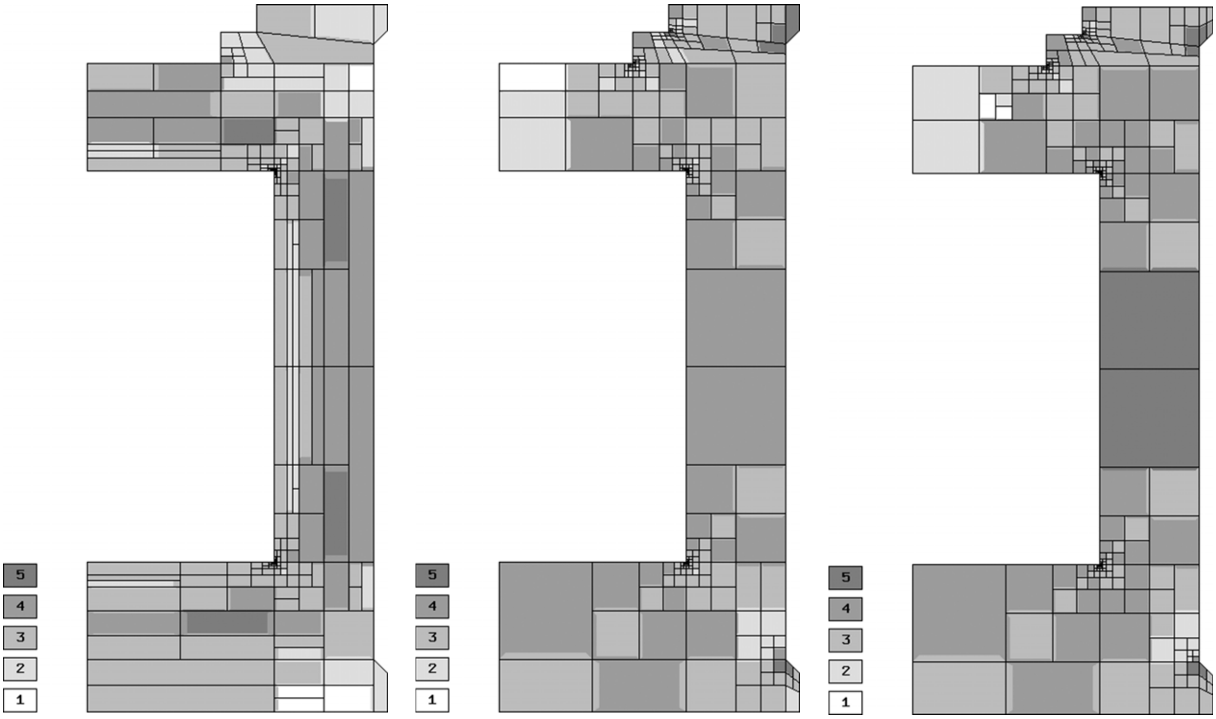


**Fig. 5.** Adaptive multimesh *hp*-FEM (temperature mesh after 1 month, 1 year, and 30 years).

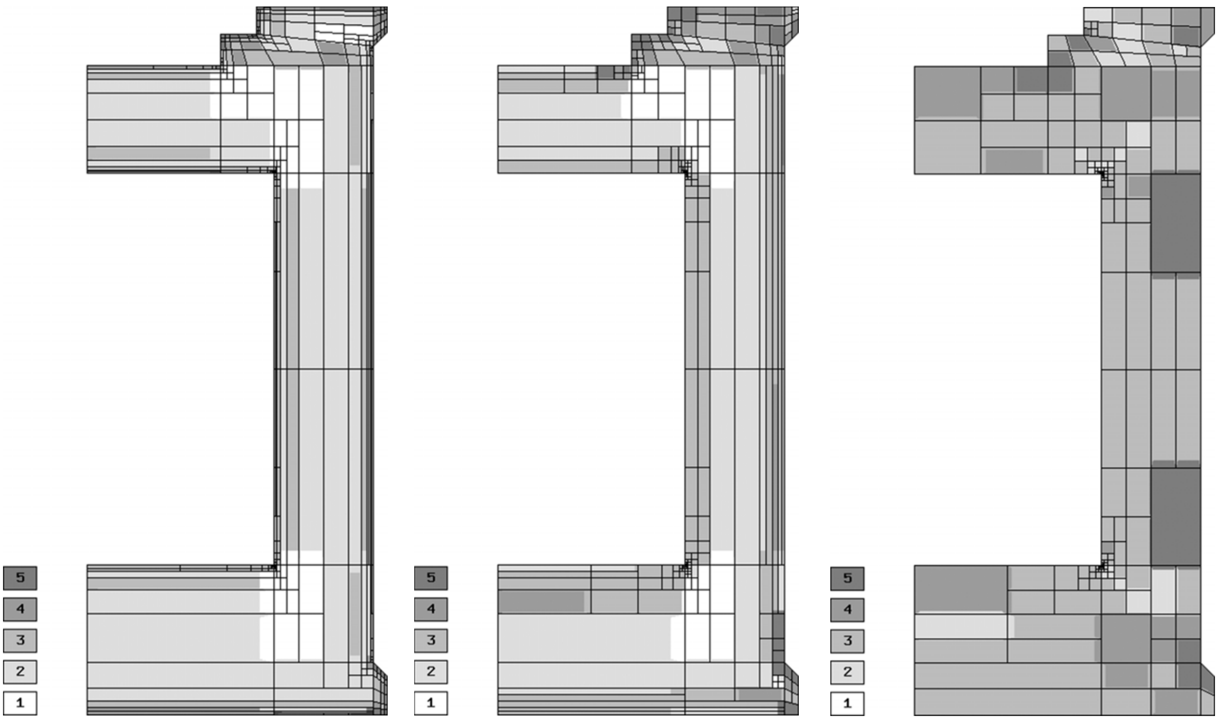


**Fig. 6.** Adaptive multimesh *hp*-FEM (moisture mesh after 1 month, 1 year, and 30 years).

independently of each other. Despite this the discretization is monolithic and no operator splitting takes place. We clearly demonstrated the superiority of the adaptive *hp*-FEM over adaptive *h*-FEM with quadratic elements. The multimesh *hp*-FEM was more efficient than the standard (single-mesh) *hp*-FEM, but we expect to see much larger differences between these two methods with more complicated multiphysics problems in the future.

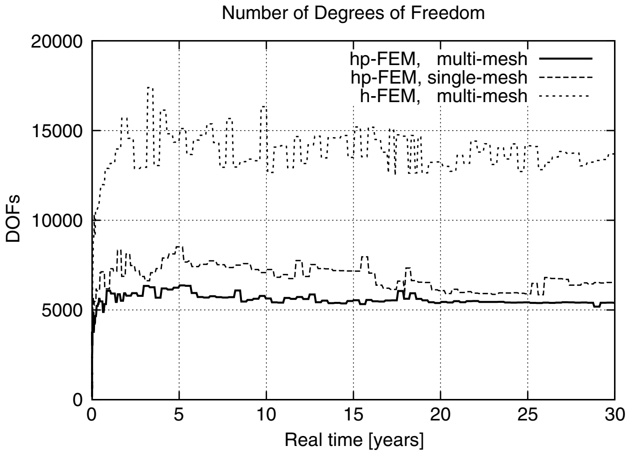


**Fig. 7.** Comparison of the three methods in terms of degrees of freedom (DOF).

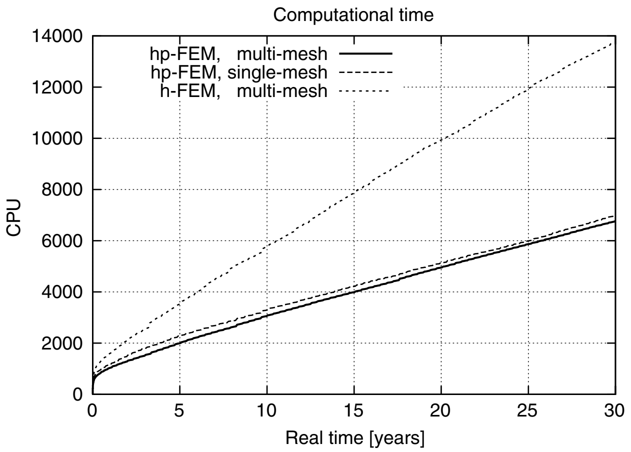


**Fig. 8.** The same comparison in terms of CPU time.

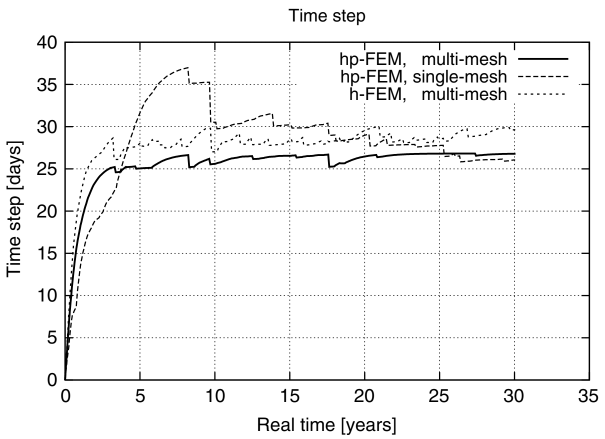


**Fig. 9.** Time step size as a function of physical time.

## Acknowledgement

The authors acknowledge the financial support of the Grant Agency of the Academy of Sciences of the Czech Republic under Project No. IAA100760702.

## References

[1] J. Kruis, T. Koudelka, Z. Bittnar, M. Petkovski, Hygro-thermo-mechanical analysis of a nuclear power plant prestressed concrete reactor vessel, in: B.H.V. Topping (Ed.), Proceedings of the Tenth International Conference on Civil, Structural and Environmental Engineering Computing, Civil-Comp Press Ltd., Stirling, Scotland, UK, 2005.
[2] R. Černý, P. Rovnaníková, Transport Processes in Concrete, Spon Press, London, 2002.
[3] R.W. Lewis, B.A. Schrefler, The Finite Element Method in the Static and Dynamic Deformation and Consolidation of Porous Media, 2nd edition, John Wiley & Sons, Ltd., Chichester, 2000.
[4] J. Kruis, Domain Decomposition Methods for Distributed Computing, Saxe-Coburg Publications, 2006.
[5] L. Dubcova, P. Solin, J. Cerveny, P. Kus, Space and time adaptive two-mesh *hp*-FEM for transient microwave heating problems, Electromagnetics (in press).
[6] P. Solin, J. Cerveny, I. Dolezel, Arbitrary-level hanging nodes and automatic adaptivity in the *hp*-FEM, Math. Comp. Simulation 77 (2008) 117–132.
[7] P. Solin, K. Segeth, I. Dolezel, Higher-Order Finite Element Methods, Chapman & Hall/CRC Press, 2003.
[8] P. Deuflhard, F. Bornemann, Scientific Computing with Ordinary Differential Equations, Springer, 2001.
[9] E. Hairer, S.P. Norsett, G. Wanner, Solving Ordinary Differential Equations, I: Non-stiff Problems, in: Springer Ser. Comput. Math., vol. 8, Springer-Verlag, Heidelberg, 1987.
[10] E. Hairer, G. Wanner, Solving Ordinary Differential Equations, II: Stiff and Differential-Algebraic Problems, in: Springer Ser. Comput. Math., vol. 14, Springer-Verlag, Heidelberg, 1991.
[11] P. Solin, J. Cerveny, L. Dubcova, D. Andrs, Monolithic discretization of linear thermoelasticity problems via adaptive multimesh *hp*-FEM, J. Comput. Appl. Math. (2009) (in press).
[12] S. Korotov, Two-sided a posteriori error estimates for linear elliptic problems with mixed boundary conditions, Appl. Math. 52 (2007) 235–249.
[13] S. Korotov, A posteriori error estimation of goal-oriented quantities for elliptic type BVPs, J. Comput. Appl. Math. 191 (2006) 216–227.
[14] P. Kus, The solution of convection-diffusion equations using adaptive higher-order methods in both space and time. Master's Thesis, Charles University, Prague, 2006.
[15] H.M. Künzel, K. Kiessl, Calculation of heat and moisture transfer in exposed building components, Int. J. Heat Mass Transfer 40 (1) (1997) 159–167.